Mathematical analysis and optimal control of heavy metals phytoremediation techniques

Lino J. Alvarez-Vázquez [a,*], Aurea Martínez [a], Carmen Rodríguez [b], Miguel E. Vázquez-Méndez [c], Miguel A. Vilar [c],

[a] *Universidade de Vigo, E.I. Telecomunicación, 36310 Vigo, Spain.*

[b] *Universidade de Santiago de Compostela, Fac. Matemáticas, 15782 Santiago, Spain.*

[c] *Universidade de Santiago de Compostela, E.P.S. Enxeñería, 27002 Lugo, Spain.*

Abstract

In this work we optimize different issues related to phytoremediation techniques for heavy metals removal from shallow water, by means of a combination of mathematical modelling, optimal control of partial differential equations and numerical optimization. We introduce, analyze and solve a 2D mathematical system of nonlinear partial differential equations representing the concentrations of heavy metals, algae and nutrients in large waterbodies. Then, we formulate an optimal control problem related to the optimization of the phytoremediation process. In particular, we determine the minimal quantity of algae to be used in the heavy metals remediation process, and locate the optimal place for such algal mass. We also propose two different full algorithms for computing the numerical solution of the control problem and, finally, we present several numerical results for a realistic case.

Key words: Mathematical modelling, Optimal control, Existence of solution, Heavy metals, Phytoremediation

* Corresponding author. Tel: +34 986 812166. Fax: +34 986 812116.
Email addresses: lino@dma.uvigo.es (Lino J. Alvarez-Vázquez), aurea@dma.uvigo.es (Aurea Martínez), carmen.rodriguez@usc.es (Carmen Rodríguez), miguelernesto.vazquez@usc.es (Miguel E. Vázquez-Méndez), miguel.vilar@usc.es (Miguel A. Vilar).

1 Introduction

Phytoremediation is one of the most usual techniques for in situ bioremediation in order to deal with environmental problems related to high concentrations of heavy metals in waterbodies. The main difficulty when operating with heavy metals pollution (mercury, lead, nickel, chromium, zinc, etc.) is due to the fact that these cannot be biodegraded once released into water. So, their indefinite persistence in the environment (and their subsequent accumulation in living organisms) can only be combated with an appropriate removal from water [1].

Phytoremediation refers to the usage of any treatment employing natural organisms (in this case plants and algae) to clean up heavy metals-contaminated water. Its main advantages are based on the effectiveness of plants to withdraw chemicals from the environment (the well-known ability of biological materials to remove and accumulate heavy metals from solutions by means of adsorption mechanisms [2]), and on their low cost when compared to other techniques (the utilization of cheap materials such as naturally abundant macroalgae and microalgae as bioadsorbents). Customary phytoremediation techniques are based on adding algal masses in regions suffering from high levels of heavy metals concentration, so that the bioadsorbent capacity of algae may reduce heavy metals contamination inside their influence area.

In order to study this environmental problem (as far as we know, unaddressed from a mathematical viewpoint), in next section we present a mathematical model for the evolution of heavy metals concentrations, set its analytical well-posedness, and introduce a computational algorithm for its numerical resolution. Then, we formulate the physical problem as a constrained optimal control problem of partial differential equations, and propose two different methods for its solution. Finally, we present several numerical examples, for a real-world case, in order to assess the efficiency of our mathematical techniques. Some of the results presented here were previously announced, for a very preliminary version of the problem, in two short notes from the authors [3,4]. In particular, in [3] a preparatory, simplified model for heavy metals concentration is proposed -although not mathematically analyzed- and in [4] a primitive formulation of the control problem is set and solved by means of a simple, naive numerical method. In the present work, following these initial steps, we state and deeply analyze a rigorous formulation of the complete problem (coupling concentrations of nutrients, algae and heavy metals in water) and propose two different sophisticated algorithms for achieving the optimal solutions that, applied in a realistic scenario, show the robustness of our approach.

2 A mathematical model

To fix ideas, let $\Omega \subset \mathbb{R}^2$ be a bounded domain (corresponding, for instance, to a lake or an estuary) representing a shallow water body, suffering from several wastewater discharges (rich in heavy metals), which causes a contamination of water surpassing the maximum admissible thresholds for heavy metals concentrations, and gives raise to sanitary problems.

We start this work by setting and analyzing a mathematical model (hat will be denoted as the state system) designed to simulate the concentration of a heavy metal in water, and to be suitable in order to indicate water quality in the domain under study Ω throughout the whole simulation time period $[0, T]$. In this study we will consider as controls (design variables in order to optimize phytoremediation techniques) the quantity $\tilde{a} \geq 0$ of added algae and the subdomain $K \subset \Omega$ where they are placed.

2.1 The state system

To formulate a mathematical model in order to simulate the evolution of heavy metal levels in a domain of shallow water, we consider the following concentrations that will be height averaged in the water column), defined to be the state variables in our problem. So, for each $x \in \Omega$ and for each $t \in [0, T]$, we consider:

- $c(x, t)$ $[g/m^3]$: the concentration of a generic heavy metal in water,
- $q(x, t)$ $[g/g]$: the concentration of heavy metal deposited in algae,
- $a(x, t)$ $[g/m^3]$: the concentration of algae in water,
- $p(x, t)$ $[g/m^3]$: the concentration of nutrients in water.

In order to model the interactions between nutrients (mainly nitrogen and phosphorus) and algae we use nonlinear convection-reaction-diffusion partial differential equations with Michaelis-Menten coupling terms [5]. In particular, for adsorption terms, the classical Lagergren model is used, which is based on a linear driving force between the concentration q of heavy metal adsorbed at time t, and the concentration of heavy metal adsorbed at equilibrium q^*, that is:

$$\frac{\partial q}{\partial t} = \kappa_q \left(q^* - q\right), \tag{1}$$

where κ_q $[1/s]$ is a first order mass transfer coefficient for adsorption rate. Moreover, in this expression, the equilibrium concentration q^* is derived from the adsorption isotherm given, for instance, by the Langmuir model:

$$q^* = \frac{Q_{max}\, b\, c}{1 + b\, c}, \tag{2}$$

where Q_{max} $[g/g]$ denotes the maximum adsorption capacity, and b $[m^3/g]$ represents an equilibrium adsorption constant related to the biosorption efficiency of algal masses.

Thus, taking into account these considerations on the interactions of nutrients, algae and heavy metals in water, above concentrations can be computed as the solution of the following system of coupled partial differential equations:

$$\frac{\partial c}{\partial t} + v \cdot \nabla c - \mu_c\, \Delta c + \kappa_c\, a\, \frac{\partial q}{\partial t} = F \quad \text{in } \Omega \times (0,T), \tag{3}$$

$$\frac{\partial q}{\partial t} = \kappa_q \left(\frac{Q_{max}\, b\, c}{1 + b\, c} - q \right) \quad \text{in } \Omega \times (0,T), \tag{4}$$

$$\frac{\partial a}{\partial t} + \tilde{v} \cdot \nabla a - \mu_a\, \Delta a - \lambda\, \frac{p}{\kappa_p + p}\, a + \gamma\, a = 0 \quad \text{in } \Omega \times (0,T), \tag{5}$$

$$\frac{\partial p}{\partial t} + v \cdot \nabla p - \mu_p\, \Delta p + \beta\, \lambda\, \frac{p}{\kappa_p + p}\, a = G \quad \text{in } \Omega \times (0,T), \tag{6}$$

with initial conditions given by:

$$c(0) = c^0, \quad q(0) = q^0, \quad p(0) = p^0 \quad \text{in } \Omega, \tag{7}$$

$$a(0) = a^0 \equiv \tilde{a}^0 + \tilde{a}\, 1_K \quad \text{in } \Omega, \tag{8}$$

and with homogeneous Neumann boundary conditions:

$$\frac{\partial c}{\partial n} = \frac{\partial a}{\partial n} = \frac{\partial p}{\partial n} = 0 \quad \text{on } \partial\Omega \times (0,T), \tag{9}$$

where

- $v(x,t) = (v_1, v_2)$ $[m/s]$ denotes water velocity (also averaged in height $h(x,t)$ $[m]$), being both variables the solution of the classical shallow water Saint-Venant equations,
- $\tilde{v}(x,t)$ $[m/s]$ represents algal velocity (for instance, in the case of immobilized algae, $\tilde{v} = 0$, and if algae move with water, $\tilde{v} = v$),
- μ_c, μ_a and μ_p $[m^2/s]$ represent the diffusion coefficients for metal, algae, and nutrient, respectively,
- κ_c is the coefficient related to mass transfer,
- λ $[1/s]$ denotes the coefficient of luminosity,
- κ_p $[g/m^3]$ represents the semi-saturation constant for nutrients,
- γ $[1/s]$ is the algal mortality rate,
- β $[g/g]$ corresponds to the nutrient-carbon stoichiometric coefficient,

- $F(x,t)$ $[g/m^3/s]$and $G(x,t)$ $[g/m^3/s]$ denote the source terms of heavy metals and nutrients, respectively,
- $1_K(x)$ is the indicator function of the region $K \subset \Omega$ where an algae mass of concentration $\tilde{a} \geq 0$ is added, at time $t = 0$, to the original concentration $\tilde{a}^0(x)$ (it is worthwhile recalling here that K and $\tilde{a}$ are intended to be the design variables of our control problem).

2.2 Mathematical analysis

In order to analyze from the mathematical viewpoint the state system (3)-(9) we will follow similar techniques to those introduced, for instance, in [6] for a different problem. So, assuming some minimal hypotheses of nonnegativeness, boundedness and regularity for initial data c^0, q^0, a^0 and p^0, for the source terms F and G, and for the velocities v and $\tilde{v}$, we will demonstrate that the state variables c, q, a and p remain nonnegative and bounded, and that they belong to a smooth enough functional space. Specifically, in our proof, we will need that the initial data c^0, q^0, a^0, $p^0 \in L^2(\Omega)$ satisfy $0 \leq c^0(x)$, $q^0(x)$, $a^0(x)$, $p^0(x) \leq M$, $\forall x \in \Omega$, the source terms $F, G \in L^2(0,T;L^2(\Omega))$ satisfy $0 \leq F(x,t)$, $G(x,t) \leq M$, $\forall (x,t) \in \Omega \times [0,T]$, and the velocities v, $\tilde{v} \in L^\infty(0,T;L^\infty(\Omega))^2$.

2.2.1 Reformulation of the State System

As a preliminary step, we rewrite the linear ordinary differential equation for q in the standard form:

$$\frac{\partial q}{\partial t} + \kappa_q q = \kappa_q \frac{Q_{max}\, b\, c}{1 + b\, c} \quad \text{in } (0,T), \qquad q(0) = q^0, \tag{10}$$

whose well-known classical solution is given by expression:

$$q(x,t) = e^{-\kappa_q t} q^0(x) + \int_0^t e^{-\kappa_q (t-s)} \kappa_q \frac{Q_{max}\, b\, c(x,s)}{1 + b\, c(x,s)} ds. \tag{11}$$

Then, taking explicit expression (11) to the partial differential equation for c, we can rewrite it in the integro-differential form:

$$\frac{\partial c}{\partial t} + v \cdot \nabla c - \mu_c \Delta c + \kappa_c\, \kappa_q\, a\, \frac{Q_{max}\, b\, c}{1 + b\, c} \tag{12}$$

$$= \kappa_c\,\kappa_q\,a\left(e^{-\kappa_q t}q^0(x) + \int_0^t e^{-\kappa_q(t-s)}\kappa_q \frac{Q_{max}\,b\,c(x,s)}{1+b\,c(x,s)}ds\right) + F$$

In order to study the existence of solution of state system (3)-(9), we use the following changes of variable:

$$c(x,t) = e^{\eta t}u(x,t), \quad a(x,t) = e^{\eta t}r(x,t), \quad p(x,t) = e^{\eta t}w(x,t), \tag{13}$$

for an arbitrary parameter $\eta > 0$. Thus, the equations for a, p and c turn into following equivalent respective expressions for r, w and u:

$$\frac{\partial r}{\partial t} + \eta r + (\gamma - \lambda\frac{w}{\kappa_p + w})\,r - \mu_a\,\Delta r = -\tilde{v}\cdot\nabla r \quad \text{in } \Omega\times(0,T), \tag{14}$$

$$\frac{\partial w}{\partial t} + \eta w - \mu_p\,\Delta w + \beta\,\lambda\,r\,\frac{w}{\kappa_p e^{-\eta t} + w} = e^{-\eta t}G - v\cdot\nabla w \quad \text{in } \Omega\times(0,T), \tag{15}$$

$$\frac{\partial u}{\partial t} + \eta u - \mu_c\,\Delta u + \kappa_c\,\kappa_q\,r\frac{Q_{max}\,b\,u}{e^{-\eta t} + b\,u} = \kappa_c\,\kappa_q\,r\left(e^{-\kappa_q t}q^0(x)\right. \tag{16}$$

$$\left. + \int_0^t e^{-\kappa_q(t-s)}\kappa_q\frac{Q_{max}\,b\,u(x,s)}{e^{-\eta s} + b\,u(x,s)}ds\right) + e^{-\eta t}F - v\cdot\nabla u \quad \text{in } \Omega\times(0,T),$$

with initial conditions:

$$r(0) = a^0, \quad w(0) = p^0, \quad u(0) = c^0 \quad \text{in } \Omega, \tag{17}$$

and boundary conditions:

$$\frac{\partial r}{\partial n} = \frac{\partial w}{\partial n} = \frac{\partial u}{\partial n} = 0 \quad \text{on } \partial\Omega\times(0,T). \tag{18}$$

Then, for the space $\tilde{B} = \{(r,w,u) \in [L^2(0,T;L^2(\Omega))]^3 \,:\, 0 \le r,w,u \le A\}$, with $A > 0$ a large enough upper bound, we define the mapping $H : (r,w,u) \in \tilde{B} \to H(r,w,u) = (\hat{r},\hat{w},\hat{u}) \in \tilde{B}$, where $(\hat{r},\hat{w},\hat{u})$ is the solution of the linear system:

$$\frac{\partial \hat{r}}{\partial t} + \eta\hat{r} + (\gamma - \lambda\frac{w}{\kappa_p + w})\,\hat{r} - \mu_a\,\Delta\hat{r} = -\tilde{v}\cdot\nabla\hat{r} \quad \text{in } \Omega\times(0,T), \tag{19}$$

$$\frac{\partial \hat{w}}{\partial t} + \eta\hat{w} - \mu_p\,\Delta\hat{w} + \beta\,\lambda\,r\,\frac{\hat{w}}{\kappa_p e^{-\eta t} + w} = e^{-\eta t}G - v\cdot\nabla\hat{w} \quad \text{in } \Omega\times(0,T), \tag{20}$$

$$\frac{\partial \hat{u}}{\partial t} + \eta\hat{u} - \mu_c\,\Delta\hat{u} + \kappa_c\,\kappa_q\,r\frac{Q_{max}\,b\,\hat{u}}{e^{-\eta t} + b\,u} = \kappa_c\,\kappa_q\,r\left(e^{-\kappa_q t}q^0(x)\right. \tag{21}$$

$$+\int_0^t e^{-\kappa_q(t-s)}\kappa_q \frac{Q_{max}\, b\, u(x,s)}{e^{-\eta s}+b\, u(x,s)} ds\Bigg) + e^{-\eta t}F - v\cdot\nabla\hat{u} \quad \text{in } \Omega\times(0,T).$$

with initial conditions:

$$\hat{r}(0)=a^0, \quad \hat{w}(0)=p^0, \quad \hat{u}(0)=c^0 \quad \text{in } \Omega, \tag{22}$$

and boundary conditions:

$$\frac{\partial \hat{r}}{\partial n}=\frac{\partial \hat{w}}{\partial n}=\frac{\partial \hat{u}}{\partial n}=0 \quad \text{on } \partial\Omega\times(0,T). \tag{23}$$

2.2.2 Some apriori estimates

First, we will obtain some estimates for the solution $(\hat{r},\hat{w},\hat{u})$ of (19)-(23). So, if we multiply equation (19) by $\hat{r}$ and integrate in $\Omega\times(0,T)$, we have:

$$\frac{1}{2}\|\hat{r}(T)\|^2_{L^2(\Omega)} + \eta\|\hat{r}\|^2_{L^2(0,T;L^2(\Omega))} + \int_0^T\int_\Omega (\gamma-\lambda\frac{w}{\kappa_p+w})\,\hat{r}^2\,dx\,dt$$
$$+\mu_a\|\nabla\hat{r}\|^2_{L^2(0,T;L^2(\Omega))^2} = -\int_0^T\int_\Omega \tilde{v}\cdot\nabla\hat{r}\,\hat{r}\,dx\,dt + \frac{1}{2}\|a^0\|^2_{L^2(\Omega)}$$

Since $w\geq 0$, then $\frac{w}{\kappa_p+w}\leq 1$ and, consequently, $\gamma-\lambda\frac{w}{\kappa_p+w}\geq\gamma-\lambda$. Thus,

$$\int_0^T\int_\Omega (\gamma-\lambda\frac{w}{\kappa_p+w})\,\hat{r}^2\,dx\,dt \geq (\gamma-\lambda)\,\|\hat{r}\|^2_{L^2(0,T;L^2(\Omega))}$$

On the other hand, by Young inequality,

$$-\int_0^T\int_\Omega \tilde{v}\cdot\nabla\hat{r}\,\hat{r}\,dx\,dt \leq \|\tilde{v}\|_{L^\infty(0,T;L^\infty(\Omega))^2}\|\nabla\hat{r}\|_{L^2(0,T;L^2(\Omega))^2}\|\hat{r}\|_{L^2(0,T;L^2(\Omega))}$$
$$\leq \|\tilde{v}\|_{L^\infty(0,T;L^\infty(\Omega))^2}\left(\frac{\epsilon}{2}\|\nabla\hat{r}\|^2_{L^2(0,T;L^2(\Omega))^2}+\frac{1}{2\epsilon}\|\hat{r}\|^2_{L^2(0,T;L^2(\Omega))}\right),$$

for any $\epsilon>0$. Choosing $\epsilon=\frac{\mu_a}{\|\tilde{v}\|_{L^\infty(0,T;L^\infty(\Omega))^2}}$ (so that $\|\tilde{v}\|_{L^\infty(0,T;L^\infty(\Omega))^2}\frac{\epsilon}{2}=\frac{\mu_a}{2}$), we derive that

$$\left(\eta+(\gamma-\lambda)-\frac{\|\tilde{v}\|^2_{L^\infty(0,T;L^\infty(\Omega))^2}}{2\mu_a}\right)\|\hat{r}\|^2_{L^2(0,T;L^2(\Omega))}+\frac{\mu_a}{2}\|\nabla\hat{r}\|^2_{L^2(0,T;L^2(\Omega))^2}\leq\frac{1}{2}\|a^0\|^2_{L^2(\Omega)}.$$

Then, for $\eta > \eta_a = \frac{\|\tilde{v}\|^2_{L^\infty(0,T;L^\infty(\Omega))^2}}{2\mu_a} - (\gamma - \lambda)$ we deduce the existence of a constant $C > 0$ such that the following estimate for $\hat{r}$ is verified:

$$\|\hat{r}\|_{L^2(0,T;H^1(\Omega))} \leq C\|a^0\|_{L^2(\Omega)}. \tag{24}$$

Now, if we multiply equation (20) by $\hat{w}$ and integrate in $\Omega \times (0,T)$, we have:

$$\frac{1}{2}\|\hat{w}(T)\|^2_{L^2(\Omega)} + \eta\|\hat{w}\|^2_{L^2(0,T;L^2(\Omega))} + \mu_p\|\nabla\hat{w}\|^2_{L^2(0,T;L^2(\Omega))^2}$$
$$+\beta\,\lambda \int_0^T\int_\Omega r\,\frac{\hat{w}^2}{\kappa_p e^{-\eta t} + w}\,dx\,dt = \int_0^T\int_\Omega e^{-\eta t} G\,\hat{w}\,dx\,dt - \int_0^T\int_\Omega v\cdot\nabla\hat{w}\,\hat{w}\,dx\,dt + \frac{1}{2}\|p^0\|^2_{L^2(\Omega)}.$$

Since $r \geq 0$, $w \geq 0$ and $e^{-\eta t} \leq 1$, then,

$$\int_0^T\int_\Omega r\,\frac{\hat{w}^2}{\kappa_p e^{-\eta t} + w}\,dx\,dt \geq 0$$

and

$$\int_0^T\int_\Omega e^{-\eta t} G\,\hat{w}\,dx\,dt \leq \|G\|_{L^2(0,T;L^2(\Omega))}\|\hat{w}\|_{L^2(0,T;L^2(\Omega))}$$

On the other hand,

$$\begin{aligned}-\int_0^T\int_\Omega v\cdot\nabla\hat{w}\,\hat{w}\,dx\,dt &\leq \|v\|_{L^\infty(0,T;L^\infty(\Omega))^2}\|\nabla\hat{w}\|_{L^2(0,T;L^2(\Omega))^2}\|\hat{w}\|_{L^2(0,T;L^2(\Omega))}\\ &\leq \|v\|_{L^\infty(0,T;L^\infty(\Omega))^2}\left(\frac{\epsilon}{2}\|\nabla\hat{w}\|^2_{L^2(0,T;L^2(\Omega))^2} + \frac{1}{2\epsilon}\|\hat{w}\|^2_{L^2(0,T;L^2(\Omega))}\right),\end{aligned}$$

for any $\epsilon > 0$. Choosing $\epsilon = \frac{\mu_p}{\|v\|_{L^\infty(0,T;L^\infty(\Omega))^2}}$ (so that $\|v\|_{L^\infty(0,T;L^\infty(\Omega))^2}\frac{\epsilon}{2} = \frac{\mu_p}{2}$), we obtain that

$$\begin{aligned}&\left(\eta - \frac{\|v\|^2_{L^\infty(0,T;L^\infty(\Omega))^2}}{2\mu_p}\right)\|\hat{w}\|^2_{L^2(0,T;L^2(\Omega))} + \frac{\mu_p}{2}\|\nabla\hat{w}\|^2_{L^2(0,T;L^2(\Omega))^2}\\ &\quad\leq \|G\|_{L^2(0,T;L^2(\Omega))}\|\hat{w}\|_{L^2(0,T;L^2(\Omega))} + \frac{1}{2}\|p^0\|^2_{L^2(\Omega)}.\end{aligned}$$

Then, for $\eta > \eta_p = \frac{\|v\|^2_{L^\infty(0,T;L^\infty(\Omega))^2}}{2\mu_p}$ we deduce the existence of a constant $C > 0$ such that the following estimate for $\hat{w}$ is verified:

$$\|\hat{w}\|_{L^2(0,T;H^1(\Omega))} \leq C(\|p^0\|_{L^2(\Omega)} + \|G\|_{L^2(0,T;L^2(\Omega))}). \tag{25}$$

Finally, arguing in a similar way with equation (21), we multiply by $\hat{u}$ and integrate in $\Omega \times (0,T)$, then:

$$\begin{aligned}
&\frac{1}{2}\|\hat{u}(T)\|^2_{L^2(\Omega)} + \eta\|\hat{u}\|^2_{L^2(0,T;L^2(\Omega))} + \mu_c\|\nabla\hat{u}\|^2_{L^2(0,T;L^2(\Omega))^2} \\
&\quad + \kappa_c\,\kappa_q \int_0^T\int_\Omega r\frac{Q_{max}\,b\,\hat{u}^2}{e^{-\eta t}+b\,u}\,dx\,dt = \kappa_c\,\kappa_q\int_0^T\int_\Omega r e^{-\kappa_q t}q^0(x)\,\hat{u}\,dx\,dt \\
&\quad + \kappa_c\,\kappa_q \int_0^T\int_\Omega r\left(\int_0^t e^{-\kappa_q(t-s)}\kappa_q\frac{Q_{max}\,b\,u(x,s)}{e^{-\eta s}+b\,u(x,s)}\,ds\right)\hat{u}\,dx\,dt \\
&\quad + \int_0^T\int_\Omega e^{-\eta t}F\,\hat{u}\,dx\,dt - \int_0^T\int_\Omega v\cdot\nabla\hat{u}\,\hat{u}\,dx\,dt + \frac{1}{2}\|c^0\|^2_{L^2(\Omega)}.
\end{aligned}$$

Again, since $0 \leq r \leq A$, $u \geq 0$, $\frac{Q_{max}\,b\,u}{e^{-\eta s}+b\,u} \leq Q_{max}$ and $e^{-\eta t} \leq 1$, then, after some simple computations:

$$\int_0^T\int_\Omega r\frac{Q_{max}\,b\,\hat{u}^2}{e^{-\eta t}+b\,u}\,dx\,dt \geq 0,$$

$$\int_0^T\int_\Omega r e^{-\kappa_q t}q^0(x)\,\hat{u}\,dx\,dt \leq A\|q^0\|_{L^2(\Omega)}\|\hat{u}\|_{L^2(0,T;L^2(\Omega))},$$

$$\int_0^T\int_\Omega r\left(\int_0^t e^{-\kappa_q(t-s)}\kappa_q\frac{Q_{max}\,b\,u(x,s)}{e^{-\eta s}+b\,u(x,s)}\,ds\right)\hat{u}\,dx\,dt \leq A\,\kappa_q\,Q_{max}\,T^{\frac{3}{2}}|\Omega|^{\frac{1}{2}}\|\hat{u}\|_{L^2(0,T;L^2(\Omega))},$$

$$\int_0^T\int_\Omega e^{-\eta t}F\,\hat{u}\,dx\,dt \leq \|F\|_{L^2(0,T;L^2(\Omega))}\|\hat{u}\|_{L^2(0,T;L^2(\Omega))},$$

and

$$\begin{aligned}
-\int_0^T\int_\Omega v\cdot\nabla\hat{u}\,\hat{u}\,dx\,dt &\leq \|v\|_{L^\infty(0,T;L^\infty(\Omega))^2}\|\nabla\hat{u}\|_{L^2(0,T;L^2(\Omega))^2}\|\hat{u}\|_{L^2(0,T;L^2(\Omega))} \\
&\leq \|v\|_{L^\infty(0,T;L^\infty(\Omega))^2}\left(\frac{\epsilon}{2}\|\nabla\hat{u}\|^2_{L^2(0,T;L^2(\Omega))^2} + \frac{1}{2\epsilon}\|\hat{u}\|^2_{L^2(0,T;L^2(\Omega))}\right),
\end{aligned}$$

Choosing now $\epsilon = \frac{\mu_c}{\|v\|_{L^\infty(0,T;L^\infty(\Omega))^2}}$ we have:

$$\left(\eta - \frac{\|v\|^2_{L^\infty(0,T;L^\infty(\Omega))^2}}{2\mu_c}\right)\|\hat{u}\|^2_{L^2(0,T;L^2(\Omega))} + \frac{\mu_c}{2}\|\nabla\hat{u}\|^2_{L^2(0,T;L^2(\Omega))^2}$$
$$\leq \kappa_c\,\kappa_q\,A\|q^0\|_{L^2(\Omega)}\|\hat{u}\|_{L^2(0,T;L^2(\Omega))} + \kappa_c\,\kappa_q^2\,A\,Q_{max}\,T^{\frac{3}{2}}|\Omega|^{\frac{1}{2}}\|\hat{u}\|_{L^2(0,T;L^2(\Omega))}$$
$$+\|F\|^2_{L^2(0,T;L^2(\Omega))}\|\hat{u}\|^2_{L^2(0,T;L^2(\Omega))} + \frac{1}{2}\|c^0\|^2_{L^2(\Omega)}.$$

Then, for $\eta > \eta_c = \frac{\|v\|^2_{L^\infty(0,T;L^\infty(\Omega))^2}}{2\mu_c}$ we deduce the existence of a constant $C > 0$ such that the following estimate for $\hat{u}$ is verified:

$$\|\hat{u}\|_{L^2(0,T;H^1(\Omega))} \leq C(1 + \|q^0\|_{L^2(\Omega)} + \|c^0\|_{L^2(\Omega)} + \|F\|_{L^2(0,T;L^2(\Omega))}). \tag{26}$$

So, taking $\eta > \eta_0 = \max\{\eta_a, \eta_p, \eta_c\}$, above estimates (24), (25) and (26) are verified.

2.2.3 Nonnegativeness and boundedness

In order to prove that $(\hat{r}, \hat{w}, \hat{u}) \in \tilde{B}$ we only need to demonstrate that $\hat{r}$, $\hat{w}$ and $\hat{u}$ are nonnegative and bounded. In this subsection, for the sake of conciseness, we will only prove it for $\hat{r}$, but the demonstrations for $\hat{w}$ and $\hat{u}$ are completely analogous (with the obvious changes).

In order to demonstrate the nonnegativeness of $\hat{r}$, we multiply equation (19) by the negative part $\hat{r}_- = \min\{\hat{r}, 0\}$ and integrate in $\Omega \times (0,t)$, for $t \leq T$. Then, arguing as in previous subsection and taking into account that by hypothesis $\hat{r}(0) = a^0 \geq 0$ (and consequently $\hat{r}_-(0) = 0$), we have:

$$\frac{1}{2}\|\hat{r}_-(t)\|^2_{L^2(\Omega)} + (\eta+\gamma)\int_0^t \|\hat{r}_-(s)\|^2_{L^2(\Omega)}ds + \mu_a\int_0^t \|\nabla\hat{r}(s)\|^2_{L^2(\Omega)^2}ds$$
$$\leq \lambda\int_0^t \|\hat{r}_-(s)\|^2_{L^2(\Omega)}ds - \int_0^t\int_\Omega \tilde{v}(s)\cdot\nabla\hat{r}(s)\,\hat{r}(s)\,ds$$
$$\leq \lambda\int_0^t \|\hat{r}_-(s)\|^2_{L^2(\Omega)}ds + \|\tilde{v}\|_{L^\infty(0,T;L^\infty(\Omega))^2}$$
$$\times\left(\frac{\epsilon}{2}\int_0^t \|\nabla\hat{r}_-(s)\|^2_{L^2(\Omega)^2}ds + \frac{1}{2\epsilon}\int_0^t \|\hat{r}_-(s)\|^2_{L^2(\Omega)}ds\right).$$

Choosing $\epsilon = \frac{\mu_a}{\|\tilde{v}\|_{L^\infty(0,T;L^\infty(\Omega))^2}}$ (so that $\|\tilde{v}\|_{L^\infty(0,T;L^\infty(\Omega))^2}\frac{\epsilon}{2} = \frac{\mu_a}{2}$), we derive that

$$\frac{1}{2}\|\hat{r}_-(t)\|^2_{L^2(\Omega)} + \left(\eta+\gamma - \frac{\|\tilde{v}\|^2_{L^\infty(0,T;L^\infty(\Omega))^2}}{2\mu_a}\right)\int_0^t \|\hat{r}_-(s)\|^2_{L^2(\Omega)}ds$$
$$+\frac{\mu_a}{2}\int_0^t \|\nabla \hat{r}_-(s)\|^2_{L^2(\Omega)^2}ds \leq \lambda\int_0^t \|\hat{r}_-(s)\|^2_{L^2(\Omega)}ds.$$

Then, for $\eta \geq \eta_a^* = \frac{\|\tilde{v}\|_{L^\infty(0,T;L^\infty(\Omega))^2}}{2\mu_a} - \gamma$,

$$\|\hat{r}_-(t)\|^2_{L^2(\Omega)} \leq 2\lambda\int_0^t \|\hat{r}_-(s)\|^2_{L^2(\Omega)}ds. \tag{27}$$

Thanks to Gronwall's Lemma, we deduce from (27) that $\|\hat{r}_-(t)\|_{L^2(\Omega)} \leq 0$, i.e., $\hat{r}_- = 0$ or, equivalently, $\hat{r} \geq 0$.

To prove that $\hat{r}$ is bounded, we need to introduce a new change of variable, defining $\tilde{r} = \hat{r} - Mt$. Denoting, for simplicity, $h(x,t) = \eta+\gamma-\lambda\frac{w}{\kappa_p+w}$, it is easy to check that $h(x,t) \geq \eta+\gamma-\lambda,\ \forall (x,t)\in\Omega\times(0,T)$ and, consequently, $h \geq 0$ if and only if $\eta \geq -(\gamma+\lambda)$. So, equation (19) can be rewritten in the equivalent form:

$$\frac{\partial \tilde{r}}{\partial t} - \mu_a\,\Delta\tilde{r} + h\tilde{r} + h\,Mt = -\tilde{v}\cdot\nabla\tilde{r} - M \quad \text{in } \Omega\times(0,T), \tag{28}$$

We multiply now equation (28) by the positive part $(\tilde{r}-M)_+ = \max\{\tilde{r}-M, 0\}$ and integrate in $\Omega\times(0,t)$. Since by hypothesis $\tilde{r}(0) = \hat{r}(0) = a^0 \leq M$, we know that $(\tilde{r}(0)-M)_+ = 0$, and we obtain:

$$\frac{1}{2}\|(\tilde{r}(t)-M)_+\|^2_{L^2(\Omega)} + \mu_a\int_0^t \|\nabla(\tilde{r}(s)-M)_+)\|^2_{L^2(\Omega)^2}ds$$
$$+\int_0^t\int_\Omega h(s)(\tilde{r}(s)-M)^2_+dx\,ds + \int_0^t\int_\Omega h(s)M(\tilde{r}(s)-M)_+dx\,ds$$
$$+\int_0^t\int_\Omega h(s)Ms(\tilde{r}(s)-M)_+dx\,ds = -\int_0^t\int_\Omega \tilde{v}(s)\cdot\nabla(\tilde{r}(s)-M)_+\,(\tilde{r}(s)-M)_+\,ds$$
$$-\int_0^t\int_\Omega M(\tilde{r}(s)-M)_+dx\,ds \leq -\int_0^t\int_\Omega \tilde{v}(s)\cdot\nabla(\tilde{r}(s)-M)_+\,(\tilde{r}(s)-M)_+\,ds$$
$$\leq \|\tilde{v}\|_{L^\infty(0,T;L^\infty(\Omega))^2}\left(\frac{\epsilon}{2}\int_0^t \|\nabla(\tilde{r}(s)-M)_+\|^2_{L^2(\Omega)^2}ds + \frac{1}{2\epsilon}\int_0^t \|(\tilde{r}(s)-M)_+\|^2_{L^2(\Omega)}ds\right).$$

Choosing again $\epsilon = \frac{\mu_a}{\|\tilde{v}\|_{L^\infty(0,T;L^\infty(\Omega))^2}}$ (as in the derivation of estimate for $\hat{r}$), for $\eta \geq \eta_a = \frac{\|\tilde{v}\|^2_{L^\infty(0,T;L^\infty(\Omega))^2}}{2\mu_a} - (\gamma - \lambda) \geq -(\gamma - \lambda)$ we have that $\|(\tilde{r}(t) - M)_+\|_{L^2(\Omega)} \leq 0$, that is, $(\tilde{r} - M)_+ = 0$ or, equivalently, $\tilde{r} \leq M$. So, from the definition of $\tilde{r}$, we obtain the bound $\hat{r} \leq M + MT = M(1+T)$.

By means of analogous arguments we can also obtain that $\hat{w}$ and $\hat{u}$ are nonnegative and bounded. Thus, $(\hat{r}, \hat{w}, \hat{u}) \in \tilde{B} = \{(r, w, u) \in [L^2(0,T;L^2(\Omega))]^3 : 0 \leq r, w, u \leq A\}$, for $A > 0$ a large enough constant, and the mapping H is well defined.

2.2.4 Existence of solution

Estimates (24), (25) and (26) for $\hat{r}$, $\hat{w}$ and $\hat{u}$, remain also valid for r, w and u. In consequence, we have:

$$\|r\|_{L^2(0,T;H^1(\Omega))} \leq C\|a^0\|_{L^2(\Omega)} = M_r,$$
$$\|w\|_{L^2(0,T;H^1(\Omega))} \leq C(\|p^0\|_{L^2(\Omega)} + \|G\|_{L^2(0,T;L^2(\Omega))}) = M_w,$$
$$\|u\|_{L^2(0,T;H^1(\Omega))} \leq C(1 + \|q^0\|_{L^2(\Omega)} + \|c^0\|_{L^2(\Omega)} + \|F\|_{L^2(0,T;L^2(\Omega))}) = M_u.$$

Thus, it is clear that the mapping H takes the set $B = \{(r, w, u) \in \tilde{B} : \|r\|_{L^2(0,T;L^2(\Omega))} \leq M_r,\ \|w\|_{L^2(0,T;L^2(\Omega))} \leq M_w,\ \|u\|_{L^2(0,T;L^2(\Omega))} \leq M_u\}$ in itself. If we consider the space $W = \{(r, w, u) \in L^2(0,T;H^1(\Omega))^3 : (\frac{\partial r}{\partial t}, \frac{\partial w}{\partial t}, \frac{\partial u}{\partial t}) \in L^2(0,T;H^1(\Omega)^*)^3\}$, we know by Aubin's Lemma that bounded sets in W are relatively compact sets in $L^2(0,T;L^2(\Omega))^3$. Then, the mapping H is compact. Consequently, by Schauder's Theorem, we deduce that H has a fixed point (r, w, u) that is a solution of system (14)-(18). Taking into account the changes of variable (13), it is straightforward that the original variables (a, p, c), solution of the system (3)-(9), also lie in $L^2(0,T;H^1(\Omega))$ and that remain nonnegative and bounded.

Finally, from the regularity achieved for c in previous subsections, we can easily obtain, from equation (10), that $q \in L^2(0,T;H^1(\Omega))$. Moreover, since by hypothesis we have that $0 \leq q^0(x) \leq M,\ \forall x \in \Omega$, we deduce by a direct computation that $0 \leq e^{-\kappa_q t} q^0(x) \leq M$ and $0 \leq e^{-\kappa_q (t-s)} \kappa_q \frac{Q_{max}\, b\, c(x,s)}{1 + b\, c(x,s)} \leq \kappa_q\, Q_{max}$, for all $x \in \Omega$ and for all $0 \leq s \leq t \leq T$. Consequently, from expression (11), we obtain that $0 \leq q(x,t) \leq M + \kappa_q\, Q_{max}\, T,\ \forall (x,t) \in \Omega \times [0,T]$, that is, q is also nonnegative and bounded.

Above results can be summarized in the following statement:

Theorem 1 *If we assume that:*

- c^0, q^0, a^0, $p^0 \in L^2(\Omega)$ *satisfy* $0 \leq c^0(x)$, $q^0(x)$, $a^0(x)$, $p^0(x) \leq M,\ \forall x \in \Omega$,

- F, $G \in L^2(0,T;L^2(\Omega))$ *satisfy* $0 \leq F(x,t)$, $G(x,t) \leq M$, $\forall (x,t) \in \Omega \times [0,T]$,
- v, $\tilde{v} \in L^\infty(0,T;L^\infty(\Omega))^2$,

then the system (3)-(9) has a solution $(c,q,a,p) \in [L^2(0,T;H^1(\Omega))]^4$ *that verifies:*

$$0 \leq c(x,t),\, q(x,t),\, a(x,t),\, p(x,t) \leq \tilde{M},\ \forall (x,t) \in \Omega \times [0,T],$$

for a suitable constant $\tilde{M} > 0$.

2.3 Numerical resolution

In order to achieve a computational solution of the state system (3)-(9), we proceed in the usual manner. We start by considering an implicit time semidiscretization of the system. Thus, we choose a natural number $N \in \mathbb{N}$, that we use to define the time step $\Delta t = \frac{T}{N}$, and we denote the discrete times $t^n = n\,\Delta t \in [0,T]$, for each $n \in \{0,\ldots,N\}$. Then, we define the approximations $c^n(x) \simeq c(x,t^n)$, $\forall n = 0,\ldots,N$, (we proceed in an analogous way for the rest of variables q^n, a^n, p^n, and for the data v^n, $\tilde{v}^n$, F^n and G^n). Therefore, starting from initial data c^0, q^0, a^0 and p^0, and defining the new parameter $\alpha = \frac{1}{\Delta t} = \frac{N}{T}$, we obtain the following system of semidiscretized, nonlinear equations posed in Ω:

$$\alpha(c^{n+1} - c^n) + v^{n+1} \cdot \nabla c^{n+1} - \mu_c\, \Delta c^{n+1} + \kappa_c\, a^{n+1}\, \alpha(q^{n+1} - q^n) = F^{n+1}, \tag{29}$$

$$\alpha(q^{n+1} - q^n) = \kappa_q \left(\frac{Q_{max}\, b\, c^{n+1}}{1 + b\, c^{n+1}} - q^{n+1} \right), \tag{30}$$

$$\alpha(a^{n+1} - a^n) + \tilde{v}^{n+1} \cdot \nabla a^{n+1} - \mu_a\, \Delta a^{n+1} - \lambda\, \frac{p^{n+1}}{\kappa_p + p^{n+1}}\, a^{n+1} + \gamma\, a^{n+1} = 0, \tag{31}$$

$$\alpha(p^{n+1} - p^n) + v^{n+1} \cdot \nabla p^{n+1} - \mu_p\, \Delta p^{n+1} + \beta\, \lambda\, \frac{p^{n+1}}{\kappa_p + p^{n+1}}\, a^{n+1} = G^{n+1}, \tag{32}$$

for $n = 0,\ldots,N-1$, completed with the homogeneous Neumann boundary conditions on $\partial\Omega$, for c^{n+1}, a^{n+1} and p^{n+1}, $n = 0,\ldots,N-1$, straightforwardly obtained from (9):

$$\frac{\partial c^{n+1}}{\partial n} = \frac{\partial a^{n+1}}{\partial n} = \frac{\partial p^{n+1}}{\partial n} = 0 \quad \text{on } \partial\Omega. \tag{33}$$

Then, for the semidiscretization in space, we employ a Lagrange P_1 finite element method (based on the use of test functions that are first-degree polynomials when restricted to each element, but globally continuous in Ω). Consequently, if we choose a mesh τ_h of Ω formed by triangular elements τ of

diameter less than h, we can approximate the Sobolev space $H^1(\Omega)$ by the finite element space $V_h = \{v_h \in \mathcal{C}(\Omega) \ : \ v_{h|\tau} \in P_1, \ \forall \tau \in \tau_h\}$.

Finally, by considering a classical variational formulation of this system of semidiscretized equations (29)-(33), the fully discretized formulation of the system can be obtained in a standard way. From this fully discretized system we are able to obtain discrete approximations of the semidiscretized functions c^{n+1}, q^{n+1}, a^{n+1}, p^{n+1}, that will be denoted as c_h^{n+1}, q_h^{n+1}, a_h^{n+1}, $p_h^{n+1} \in V_h$, respectively.

From a computational viewpoint, the nonlinearities appearing in this variational formulation will be solved by using an iterative fixed-point algorithm. With respect to the iterative process, we start the resolution by iterating first in variable p_h^{n+1}, then in variable a_h^{n+1}, and finally in variable c_h^{n+1}. Now, once computed the approximations p_h^{n+1}, a_h^{n+1} and c_h^{n+1}, the last variable q_h^{n+1} is updated by a straightforward rewriting of the semidiscretized equation (30) in the explicit way:

$$q_h^{n+1} = \frac{1}{\alpha + \kappa_q} \left(\alpha \, q_h^n + \kappa_q \, \frac{Q_{max} \, b \, c_h^{n+1}}{1 + b \, c_h^{n+1}} \right). \tag{34}$$

3 The optimal control problem

As remarked in previous sections, we are aimed to find the optimal location K of the algal mass to be added and the minimal quantity $\tilde{a}$ of algae, such that the water quality (measured by means of the solution of the state system (3)-(9)) is optimized. This environmental problem can be formulated as a control-constrained optimal control problem, so that it can be analyzed by using techniques related to those already employed by the authors in other environmental scenarios as can be found, for instance, in previous papers [7–9].

In this formulation of the problem, the control $(K, \tilde{a})$ enters the state system (3)-(9) *via* the variable a, specifically through its initial condition (8). So, regarding the first control K, taking into account geopolitical reasons, we will impose a few constraints related to the feasible locations of the mass of algae. In particular, area K will be constructed from an origin point p that we will assume inside an admissible region $\mathcal{K}_{ad} \subset \Omega$. Thus, the algal region K is composed by the triangle where the central point p lies and also the three adjacent triangles (in this way, the region K takes the form of a "triangular" surface composed by four contiguous finite elements of the mesh, constructed from the actual design variable p). With respect to the second control variable $\tilde{a}$, that is nonnegative from definition, we will ask it not to exceed an upper threshold

$A_{max} > 0$, determined from economic and technological motivations. In a few words, we are assuming the following constraints on the control variables:

$$p \in \mathcal{K}_{ad}, \qquad \tilde{a} \in [0, A_{max}]. \tag{35}$$

With respect to the objective function J to be minimized, we will take, for example, the concentration of heavy metals inside a "sensitive" region $S \subset \Omega$ (which can be even the whole domain Ω), needing to be protected against heavy metals contamination. In this way, the simplest example of cost functional to be optimized can be written, for instance, under the form:

$$J(p, \tilde{a}) = \int_0^T \int_S c(x,t)\, dx\, dt \tag{36}$$

where $c(x,t)$ is given by the solution of the state system (3)-(9), with the initial condition a^0 corresponding to control $(K, \tilde{a})$, actually defined from the design variables $(p, \tilde{a})$. Further possible choices for alternative objective functions J can be found in the numerical tests presented in below section).

Thus, the control-constrained optimal control problem to be solved corresponds to find the optimal location K and amount $\tilde{a}$ of algae to be added such that verify the associated state system (3)-(9), satisfy the control constraints (35) and minimize the objective function J. Therefore, the problem can be written is a shortened form as:

$$\min_{\substack{p \in \mathcal{K}_{ad} \\ 0 \leq \tilde{a} \leq A_{max}}} J(p, \tilde{a}) \tag{37}$$

where $\mathcal{K}_{ad}$ and A_{max} are known data.

In order to solve this optimal control problem, we propose two different approaches. The former (naiver) approach uses the program *Heavy metals* of the 2D finite volume hydrodynamic model MIKE 21 [10], developed by the Danish Institute of Technology (DHI). For optimization purposes, given the essentially geometric nature of the problem, the authors propose to use a direct search algorithm: the Nelder-Mead simplex method [11]. This derivative-free algorithm has been successfully used by the authors in other related environmental problems (see, for instance, previous work [12], where a short description of the method can be also found), and presents good convergence properties in low dimensions (it is immediate to check that in our problem the design variable $(p, \tilde{a}) \in \mathbb{R}^3$). However, since Nelder-Mead algorithm was originally designed for unconstrained minimization problems, in order to apply it to the control-constrained optimization problem (37) we need first to modify our

cost function J by adding a penalty term related to the fulfilling of the control constraints (35), which can be made in a simple and standard way.

The latter (alternative) approach is developed by using the open-source finite element software Freefem++ [13], through a full programming of the algorithms presented in above Subsection 2.3. Moreover, to solve the nonlinear optimization problem (37), the use of the interior-point algorithm IPOPT [14] is proposed. This is an interior-point filter line-search method especially intended for nonlinear programming of large-scale problems, which can be interfaced with the Freefem++ code. In the optimization procedure, the computation of the necessary cost gradients is approximated by a finite difference scheme. It is worthwhile saying in advance that the results obtained from both approaches have been completely similar, both from a qualitative and from a quantitative point of view, which assures the robustness of our methodology.

4 Computational results

This concluding section presents some numerical tests for a real-world scenario posed in the estuary *Ría de Vigo* (Galicia, NW Spain), particularly in the region surrounding Cangas harbour. The case shown here corresponds to a known wastewater discharge from a small number of shipyards located in the area, which shows a high concentration of lead. For the phytoremediation process, the native green alga *Ulva* -commonly known as *sea lettuce*- was used as a bioadsorbent.

For the computational experience presented here, the numerical results have been achieved through the two different, above commented approaches. For the sake of conciseness, from the large set of numerical tests developed to analyze the effects of the presence of an algal mass in the surroundings of the given discharge point, only a few figures are shown and commented here.

4.1 A gradient-free approach

In this approach, we combine the application of the finite volume software MIKE 21, widely employed in the study of environmental problems, with our own code for the Nelder-Mead algorithm (modified with an oriented restarting when stagnation at a non-optimal point is detected).

In the numerical experiment presented here, we have chosen as cost function J the mean concentration of heavy metals in water inside the sensitive region S, that is:

$$J(p,\tilde{a}) = \frac{1}{T\,|S|}\int_0^T\int_S c(x,t)\,dx\,dt \tag{38}$$

where $|S|$ denotes the Euclidean measure of set S. Moreover, for the control constraints in the optimization process, the feasible region $\mathcal{K}_{ad}$ is given by a rectangular area centered in the wastewater discharge point, and the upper threshold for added algae is taken as $A_{max} = 60.00\,g/m^3$.

So, in this computational test, we start from a set of four initial random simplices:

$$(p_1,\tilde{a}_1) = ((518376.99, 4677839.17), 20.00),$$
$$(p_2,\tilde{a}_2) = ((518587.76, 4677845.97), 25.00),$$
$$(p_3,\tilde{a}_3) = ((518465.38, 4678070.33), 15.00),$$
$$(p_4,\tilde{a}_4) = ((518492.57, 4677920.76), 30.00),$$

whose cost values range from $J = 9.1250\ 10^{-4}$ to $J = 9.4375\ 10^{-4}$. Then, after 173 cost function evaluations, we arrive to the optimal control:

$$(p,\tilde{a}) = ((518864.62, 4677937.99), 59.99),$$

where the objective function takes now the optimized value $J = 6.9125\ 10^{-4}$ (which represents a reduction in lead concentration of almost a 25% with respect to the best uncontrolled situation).

The four figures included here correspond to zooms on the area of interest in the *Ría de Vigo* (region of the harbour of Cangas). So, Figure 1 shows the lead concentration c at high tide, after two complete tidal cycles (about $T = 24.8$ hours) for the initial (uncontrolled) configuration, obtained by the numerical resolution of the problem in a spatial triangular mesh τ_h of 1941 elements and 1129 vertices, with a time step $\Delta t = 30\,s$. We can appreciate here the protected area (formed by two regions delimited by a white thick line), and the original location K for algae (region composed of four triangles depicted by a white thin line). Figure 2 shows the heavy metal concentration c, at same final time, for the optimized (controlled) configuration, where the optimal location K is now depicted by a coloured thick line. Figures 3 and 4 show lead concentrations c at low tide, for the uncontrolled and the controlled configurations, respectively.

After a direct visual comparison of these pictures, we can easily appreciate the differences between the original (uncontrolled) mass of *Ulva* in the discharge zone (Figures 1 and 3) and the optimized addition of an algal mass in that zone (Figures 2 and 4). We can notice in these graphics how the lead concentration in water is considerably diminished by adding the optimal amount of algae in

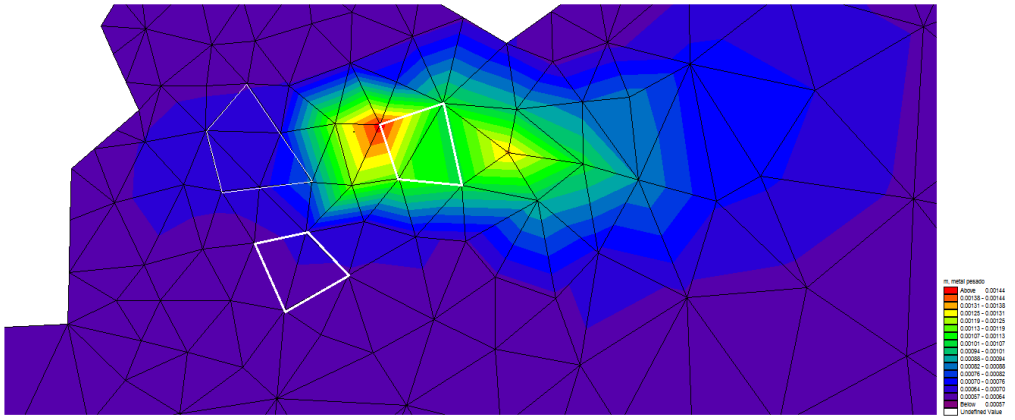

Fig. 1. Levels of lead concentration in water at high tide, for the uncontrolled situation posed in a part of the estuary *Ría de Vigo*. The discharge zone corresponds to the black point on the left side of the peak of concentration, the protected areas S are depicted by white thick lines, and the initial algae location K is delimited by a white thin line.

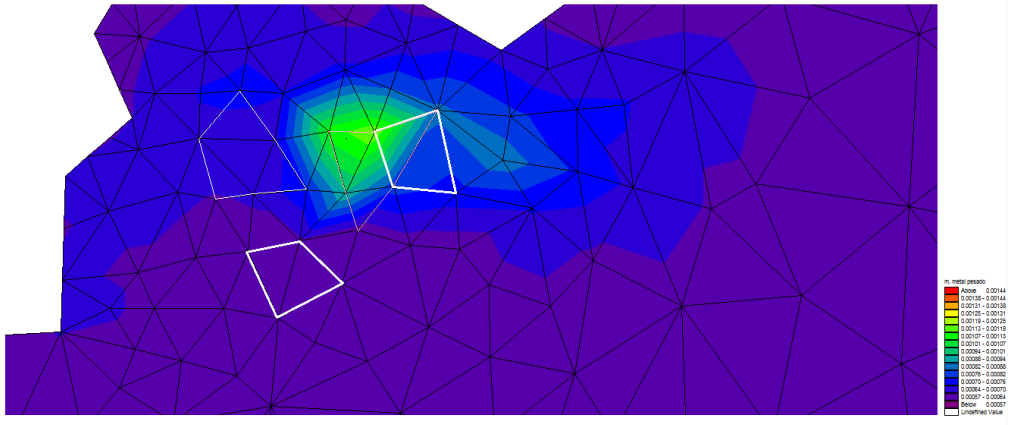

Fig. 2. Levels of lead concentration in water, corresponding to the same scenario, after the controlled placement of a mass of algae $\tilde{a} = 59.99\, g/m^3$ in the optimal area K depicted by a coloured thin line. The discharge point can be clearly seen close to the peak of concentration.

the optimal region near the source of pollution (black point close to the most highly contaminated vertex in Figures 1 to 4).

We must note here how the tidal movement affects to the propagation of pollution: when approaching high tide, water moves to the right and consequently heavy metal moves so. However, at low tide period, water moves to the left and accordingly heavy metal moves in the same direction. It is also important to notice how the reduction of lead concentration is not only restricted to the particular area where the algal mass is placed, but it also expands to the surrounding regions of the estuary, essentially due to the natural movement of water by the tide effect.

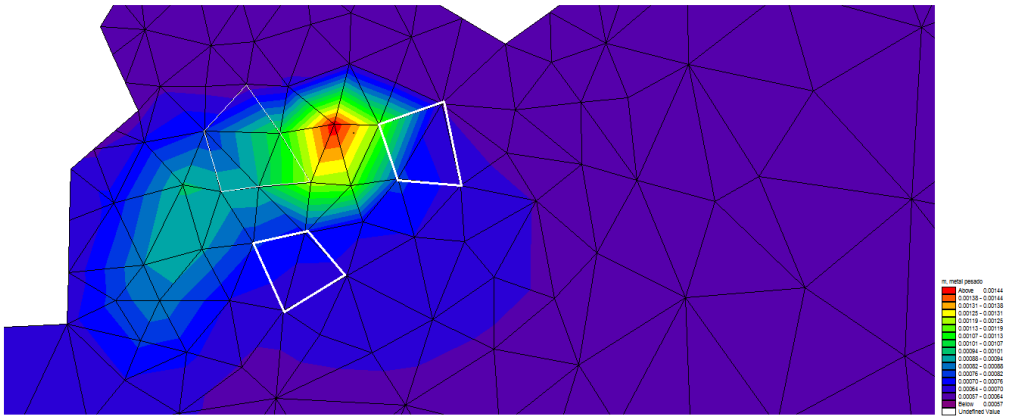

Fig. 3. Levels of lead concentration in water at low tide, for the uncontrolled situation posed in a part of the estuary *Ría de Vigo*. The discharge zone corresponds to the point on the right side of the peak of concentration, the protected areas S are depicted by white thick lines, and the initial algae location K is delimited by a white thin line.

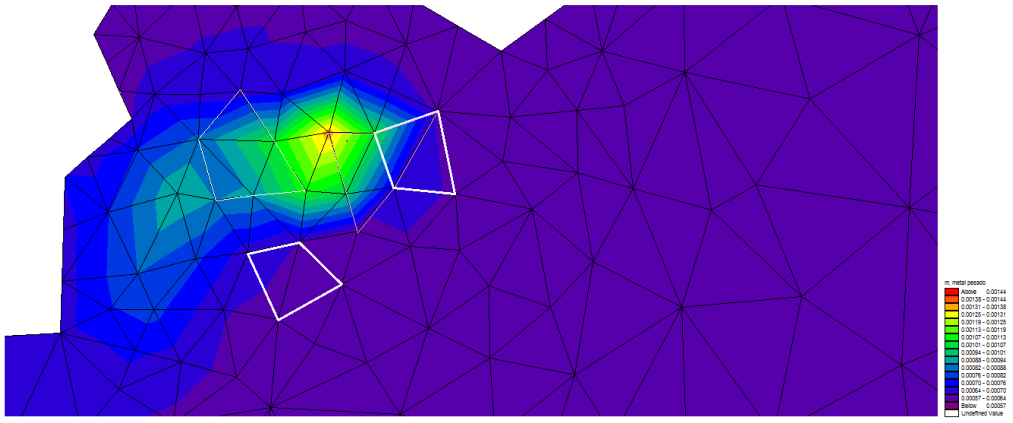

Fig. 4. Levels of lead concentration in water, corresponding to the same scenario, after the controlled placement of a mass of algae $\tilde{a} = 59.99\, g/m^3$ in the optimal area K depicted by a coloured thin line.

Finally, from a quantitative point of view, we can observe how -in absence of other additional constraints as, for instance, those related to the economic cost of the processes or to technological restriction- the optimized quantity of added algae $\tilde{a} = 59.99\, g/m^3$ approaches the maximum allowed quantity $A_{max} = 60.00\, g/m^3$ (because the larger the quantity of algae, the more intense the bioremediation effects and then, as there are no other restrictions, the optimal amount of added algae is at its maximum level). Moreover, we can also notice how, as might be expected, the optimal region K moves closer to the upper half of the protected region S and also to the wastewater discharge point, in order to intensify phytoremediation effects (since the lower half of the protected area S is farther from the discharge point and, consequently, it is much less affected by lead emissions than the upper half).

4.2 An alternative interior-point approach

Among all the numerical tests developed under this approach (i.e., obtained by means of the code Freefem++ interfaced with the IPOPT algorithm), we only present here a pair of figures. These graphics correspond to a new example posed in the scenario presented in previous approach (with same model data and parameters), including only two differences. The first difference is associated to the definition of the cost function: in this approach we choose J as the mean concentration of heavy metal in protected region S at final time T, that is:

$$J(p, \tilde{a}) = \frac{1}{|S|} \int_S c(x, T)\, dx, \tag{39}$$

The second difference is connected to the control constraints: the feasible region $\mathcal{K}_{ad}$ is the same rectangle surrounding the discharge point, but the upper threshold for the algal mass is expanded to $A_{max} = 80.00\, g/m^3$.

For the minimization procedure, we start from an initial random point:

$$(p_1, \tilde{a}_1) = ((518684.26, 4677554.95), 20.00),$$

whose objective value is $J = 7.0318\ 10^{-4}$. Then, after 8 iterations of the interior-point algorithm (that correspond to 9 evaluations of the cost function and its gradient), we arrive to the optimal point:

$$(p, \tilde{a}) = ((518711.88, 4677554.95), 79.99),$$

where the cost function now drops down to $J = 5.1327\ 10^{-4}$ (which means an effective reduction in lead concentration of more than a 27% with respect to the initial arbitrary case).

Both figures presented here show the whole *Ría de Vigo* (suffering from the same lead discharge in the region of Cangas harbour as in previous example). In particular, Figure 5 depicts, for the whole domain Ω, lead concentration c after two complete tidal cycles corresponding to the uncontrolled configuration, as computed by means of the numerical resolution of the state system (3)-(9) with initial condition constructed from initial random point $(p_1, \tilde{a}_1)$. Figure 6 represents the lead concentration c, at same time as above, for the optimized configuration. In this case, we can clearly appreciate the discharge point, that corresponds to the small area with the maximum concentration of lead, and also the optimal location K, that corresponds to the region, close to

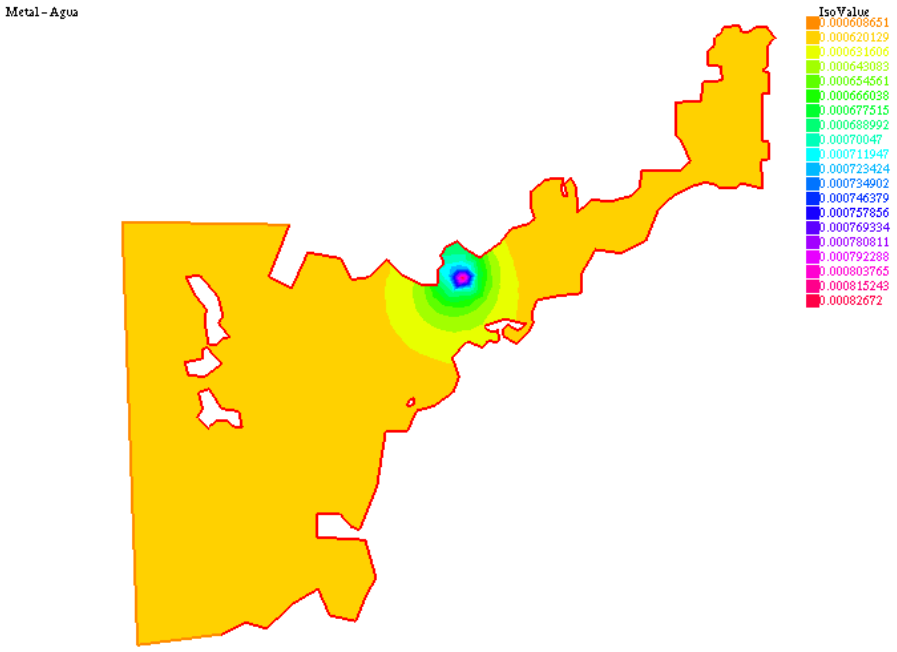

Fig. 5. Whole representation of the lead concentration in water for the uncontrolled situation posed in the estuary *Ría de Vigo*, once two tidal cycles have passed.

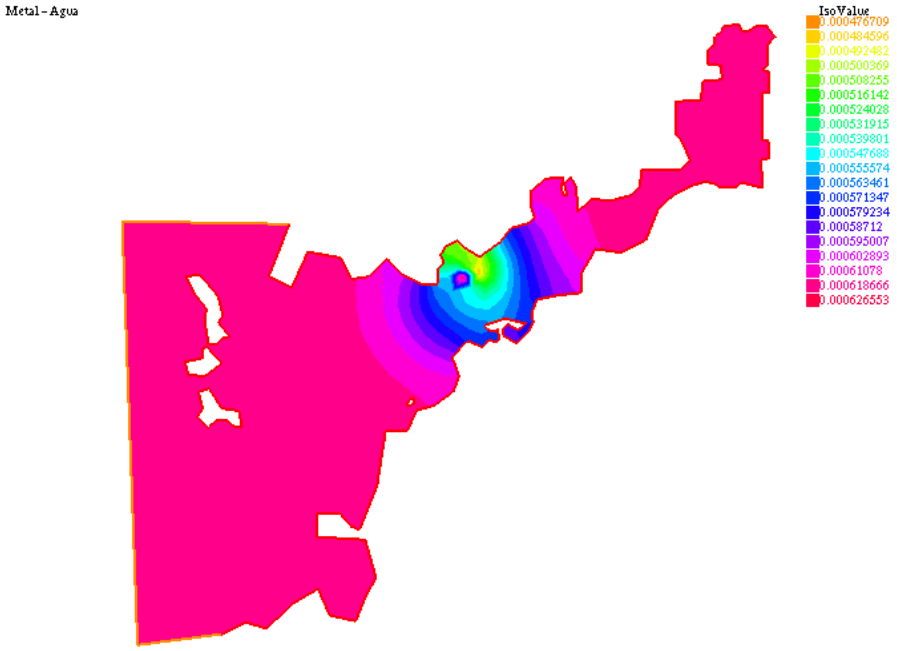

Fig. 6. Concentration of lead in water for the same scenario, after the optimized placement of an algal mass $\tilde{a} = 79.99\, g/m^3$ in the optimal area K. The discharge point corresponds to the peak of concentration, and the optimal location K is the region (near to the discharge point) where lead concentration takes lowest values.

the discharge point, with the minimum lead concentration. We can also appreciate here the discharge zone, corresponding to the region with the maximum concentration of lead. Again, despite the different colour scales, a striaightforward comparison of both figures shows us the clear differences between the lead concentrations obtained in both cases for the whole region Ω.

Finally, although the figures for the first example (Figures 1 to 4) are focused only in the region of interest and the figures for the second example (Figures 5 and 6) show the whole domain, we can appreciate that the solutions achieved from both approaches are completely similar both from the qualitative and the quantitative point of view, which assesses the accurateness of our methodology. Consequently, the remarks from above subsection on the reduction of lead concentration and on the behaviour of optimal controls remain also valid for this second approach. Specifically, the optimized region K also approaches the protected region and the discharge point (by the reasons already commented), and the optimal quantity of algae $\tilde{a} = 79.99\, g/m^3$ tends to the maximum threshold $A_{max} = 80.00\, g/m^3$, since no further constraints are imposed.

5 Conclusions and future work

In this paper, we present an optimal control approach to phytoremediation techniques for heavy metals removal from water. First, a novel formulation of the problem has been introduced and fully analyzed from a theoretical viewpoint. The considered systems describe the evolution of concentrations of nutrients, algae and heavy metals in water, in order to optimize phytoremediation methods. Here we have focused on only two (albeit very important) aspects of the phytoremediation process: the minimal quantity of algae to be added in the procedure and the optimal location of this mass of algae. However, our methodology can be straightforwardly applied to study other related issues as, for instance, the determination of the optimal time of residence of algae to optimize heavy metals removal, or the minimization of the total economic cost of the process. We have also proposed two numerical algorithms for computing the optimized phytoremediation techniques. In addition, through a realistic test example, the effectiveness and usefulness of our approach were confirmed, showing that, in our particular case, the removal of heavy metals from water could be improved more than a 25% by employing the optimized configuration.

Although the mathematical analysis of the modelling system is fully developed in the first part of the paper, the study of the optimal control problem remains still partially open (in particular, the interesting point related to obtaining

optimality conditions in order to achieve a theoretical characterization of the optimal solutions). The reason for this shortcoming may be the strongly nonlinear nature of the elements defining the optimal control problem. A deeper research on these issues should be developed as part of any future work.

Acknowledgments

The authors thank the funding from project MTM2015-65570-P of MINECO/FEDER (Spain). The support provided by DHI with modelling system MIKE21 is also greatly appreciated. The authors would like to acknowledge the reviewers and editors whose comments have greatly improved this manuscript.

References

[1] D. Mani, C. Kumar, Biotechnological advances in bioremediation of heavy metals contaminated ecosystems: An overview with special reference to phytoremediation, Int. J. Environ. Sci. Technol. 11 (2014) 843–872.

[2] H. Perales-Vela, J. Peña-Castro, R. Cañizares-Villanueva, Heavy metal detoxification in eukaryotic microalgae, Chemosphere 64 (2006) 1–10.

[3] A. Martínez, L.J. Alvarez-Vázquez, C. Rodríguez, M.E. Vázquez-Méndez, M.A. Vilar, Heavy metals phytoremediation: First mathematical modelling results, in: F.A. Radu et al. (Eds.), Numerical Mathematics and Advanced Applications ENUMATH 2017, Springer, 2019, pp. 819–827.

[4] L.J. Alvarez-Vázquez, A. Martínez, C. Rodríguez, M.E. Vázquez-Méndez, M.A. Vilar, Optimal control of phytoremediation techniques for heavy metals removal in shallow water, in: H.C. Rodrigues et al. (Eds.), EngOpt 2018 Proceedings of the 6th International Conference on Engineering Optimization, Springer, 2019, pp. 352–360.

[5] L.J. Alvarez-Vázquez, F.J. Fernández, R. Muñoz-Sola, Mathematical analysis of a three-dimensional eutrophication model, J. Math. Anal. Appl. 349 (2009) 135–155.

[6] E. Casas, C. Ryll, F. Troltzsch, Sparse optimal control of the Schlogl and FitzHugh-Nagumo systems, Comput. Meth. Appl. Math. 13 (2013) 415–442.

[7] L.J. Alvarez-Vázquez, A. Martínez, R. Muñoz-Sola, C. Rodríguez, M.E. Vázquez-Méndez, The water conveyance problem: Optimal purification of polluted waters, Math. Models Meth. Appl. Sci. 15 (2005) 1393–1416.

[8] L.J. Alvarez-Vázquez, F.J. Fernández, A. Martínez, Optimal management of a bioreactor for eutrophicated water treatment: A numerical approach, J. Sci. Comput. 43 (2010) 67–91.

[9] L.J. Alvarez-Vázquez, A. Martínez, C. Rodríguez, M.E. Vázquez-Méndez, Sediment minimization in canals: An optimal control approach, Math. Comput. Simul. 149 (2018) 109–122.

[10] MIKE 21, User guide and reference manual, Danish Hydraulic Institute, Horsholm, 2001.

[11] J.A. Nelder, R. Mead, A simplex method for function minimization, Computer J. 7 (1965) 308–313.

[12] L.J. Alvarez-Vázquez, A. Martínez, C. Rodríguez, M.E. Vázquez-Méndez, Numerical optimization for the location of wastewater outfalls, Comput. Optim. Appl. 22 (2002) 399–417.

[13] F. Hecht, New development in Freefem++, J. Numer. Math. 20 (2012) 251–265.

[14] A. Wächter, L.T. Biegler, On the implementation of an interior-point filter line-search algorithm for large-scale nonlinear programming, Math. Program. 106 (2006) 25–57.